applied sciences

MDPI

Article

A Study of the Bond Strength and Mechanism between Basalt Fibers and Asphalt Binders

Zhiwei Sun [1], Changjiang Kou [1,2,*], Yu Lu [1], Zhengguang Wu [1,2], Aihong Kang [1,2] and Peng Xiao [1,2]

[1] College of Civil Science and Engineering, Yangzhou University, Yangzhou 225127, China; sun_zhiwei_yzu@163.com (Z.S.); yzuluyu1009@163.com (Y.L.); zgwu@yzu.edu.cn (Z.W.); kahyzu@163.com (A.K.); xpyzu@163.com (P.X.)

[2] Research Center for Basalt Fiber Composite Construction Materials, Yangzhou 225009, China

* Correspondence: changjiang.kou@yzu.edu.cn

Abstract: The bond strength between basalt fibers and asphalt binders is an important parameter that can be used to evaluate the influence of basalt fibers on the mechanical properties of asphalt binders and asphalt mixtures. To date, however, there remains a lack of methods that can be used to assess the bond strength between basalt fibers and asphalt binders. This study employed a fiber-asphalt pull-out tester (POT). Significant upward, peak, and downward stages were observed from the relationship curves between the pull-out force (POF) and displacement, corresponding to the holding stage and reaching the maximum POF stage and the sliding or failure stage between fibers and asphalt binders. Maximum POF is recommended to calculate the bond strength between basalt fibers and asphalt binders. The types of asphalt binders suitable for basalt fibers and the appropriate fiber embedding depths for different types of asphalt binders guiding the selection of fiber length are recommended based on the influence of fiber embedding depth and asphalt binders on the fiber–asphalt bond strength. In addition, surface energy was used to calculate the bond strength as well. Surface energy was determined from contact angle measurements using the sessile drop method. Furthermore, a scanning electron microscope (SEM) was employed to examine the bond mechanism between asphalt binders and basalt fibers. These experiments showed how basalt fibers serve to reinforce asphalt mixtures by bonding with asphalt binders.

Keywords: asphalt binder; basalt fiber; pull-out tester; bond strength; bond mechanism

check for updates

Citation: Sun, Z.; Kou, C.; Lu, Y.; Wu, Z.; Kang, A.; Xiao, P. A Study of the Bond Strength and Mechanism between Basalt Fibers and Asphalt Binders. *Appl. Sci.* **2024**, *14*, 2471. https://doi.org/10.3390/app14062471

Academic Editor: Giuseppe Lacidogna

Received: 23 February 2024
Revised: 11 March 2024
Accepted: 11 March 2024
Published: 14 March 2024

Copyright: © 2024 by the authors. Licensee MDPI, Basel, Switzerland. This article is an open access article distributed under the terms and conditions of the Creative Commons Attribution (CC BY) license (https://creativecommons.org/licenses/by/4.0/).

1. Introduction

Hot mixture asphalt (HMA) is one of the essential materials used for the construction of asphalt pavements in road engineering worldwide [1,2]. However, distresses such as rutting, cracks, potholes, looseness, and so on occur frequently in asphalt pavement due to increases in traffic loading and severe environmental factors [3–5]. Therefore, it is of great importance to find ways to strengthen the performance of HMA. Many researchers and agencies strive to develop new mineral gradations [6] to improve the performance of raw materials, including aggregates, asphalt binders, and additives [7–9]. In recent years, fibers have been employed to enhance the performance of HMA in heavy-duty road pavement [10]. Li, Z. et al. used basalt fibers to enhance the low-temperature performance of asphalt mixtures in heavily frozen areas and found that the low-temperature failure type of asphalt mixtures changed from brittle failure to flexible failure at −20 °C [11]. Davar A. introduced the use of basalt fibers in reinforced mixtures and found that basalt fibers compensated for the weaknesses of asphalt mixtures at lower temperatures [12]. Katkhuda, H. et al. reported that basalt fibers enhanced the compressive strength of a concrete specimen and improved its flexural and splitting tensile strength [13,14].

Basalt fibers are typical inorganic, environmentally friendly fibers with good tensile strength, showing higher adhesion to asphalt binders than other fibers. To date, the influence of the content and lengths of basalt fibers on the performance of basalt-fiber-reinforced

HMA (BF-HMA) has been systematically studied by many researchers. Xie, X. et al. prepared basalt fiber asphalt samples with three lengths (3, 6, and 9 mm) and four proportions (0%, 3%, 6%, and 9%, according to the weight of asphalt binders) [15]. The comprehensive strength of asphalt mastics was the best with a fiber length of 6–9 mm and a fiber content of 3–6%. Gu, Q. et al. experimentally determined that the recommended basalt fiber content was 2% by weight of asphalt binder based both on dispersion and rheological properties [16]. The recommended basalt fiber length was 9 mm. Lou K. selected different lengths (3, 6, 9, 12, and 15 mm) of BF and then prepared HMA samples using mixed-length BFs [17]. The results showed that mixed-length BFs greatly improved the overall performance of HMA. Qin, X. et al. suggested that the optimum length of basalt fibers is 6 mm and that the optimum content is 5–7% according to the weight of asphalt mastics [18,19]. Kathari, P.M. et al. compared an asphalt binder reinforced with basalt fibers to an asphalt binder without fibers. The dosages of basalt fiber used in the study were 0.5%, 1.0%, 1.5%, 2.0%, and 2.5% by weight of the asphalt binder. Basalt asphalt binder provided better crack resistance, especially at high temperatures. In addition, it was found that the performance of the binder could only be significantly improved with a fiber dosage of 1% [20].

Lou, K. et al. discovered that the tensile strength of asphalt–fiber mastics increased because the basalt fibers carried part of the tensile load [21]. This increase in tensile strength implied that there was good adhesion between the asphalt and fibers. Wu, B. et al. studied basalt fibers for asphalt mastic deformation resistance, high-temperature performance, and low-temperature performance [22]. The results showed that the fibers improved the deformation resistance of the asphalt mastic. The morphology of the fibers affected the rheological properties of fiber asphalt mastic and changed its mechanism. Wang, D. et al. investigated the effect of basalt fibers on asphalt binders and mastics at low temperatures. The fatigue resistance of an asphalt binder enhanced by basalt fibers was evaluated [23]. The test results indicated that the tensile strength and fatigue life of asphalt binder can be significantly improved by using an appropriate content of basalt fibers. Fu, Z. et al. comprehensively characterized the rheological properties of modified asphalt binders. The rheological properties were analyzed using tools such as a Dynamic Shear Rheometer (DSR) [24]. According to the test results, the optimal amount of modifier was changed to 4%, and the optimal amount of basalt fiber was changed to 6%. In some special cases, the content of modifiers can be changed appropriately. Cheng, X. et al. tested and evaluated six silane coupling agents for modifying the rheological properties of basalt-fiber-reinforced asphalt at different elevated temperature conditions and detailed the correlation between surface components and rheological properties in terms of temperature response [25]. The cited study provided guidance on the use of silane coupling agents in combination with mineral fillers to improve the overall performance of asphalt mixtures.

Mohammed, M. et al. described how the pneumatic adhesion tensile testing instrument (PATTI) was used to examine the mechanism by which fibers influence the pull-off tensile strength of asphalt mastics [26]. The results showed that fibers led to an increased pull-off tensile strength of the mastics and changed the failure mode from cohesive to hybrid, implying an improvement in the cohesive strength of the mastic. Rahim, A. et al. developed the compression pull-off test (CPOT) to study the cohesive and adhesive bond strength of binders [27]. They concluded that the COPT was useful for investigating the phenomenon of cavitation and fibrillary concentration in the cohesive bonds of asphalt and mastics. Most investigations show that it is the bond strength between basalt fibers and asphalt binders that determines the performance of basalt fiber-reinforced asphalt mixtures [28,29]. The literature on basalt fiber asphalt binders has highlighted several properties, such as high- and low-temperature rheological properties [30], crack resistance [31], shear resistance [32], fatigue performance [33], and so on.

However, there is still a lack of easily performable approaches that can be used to assess the bond strength between basalt fibers and asphalt binders. This study aimed to develop a fiber–asphalt binder bond strength tester and evaluate the influence of the embedment depths of basalt fibers and asphalt binders on bond strength. Additionally, the

adhesion mechanism between basalt fibers and asphalt binders was studied by using a scanning electron microscope and the contact angle test.

2. Materials and Methods

2.1. Raw Materials

2.1.1. Fiber

Basalt fibers (BFs), as shown in Figure 1, with a golden-brown appearance and a smooth, straight surface were adopted in this experiment. The fiber diameter was 16 µm, and the fiber width was 1.589 cm. The properties of BFs are presented in Table 1.

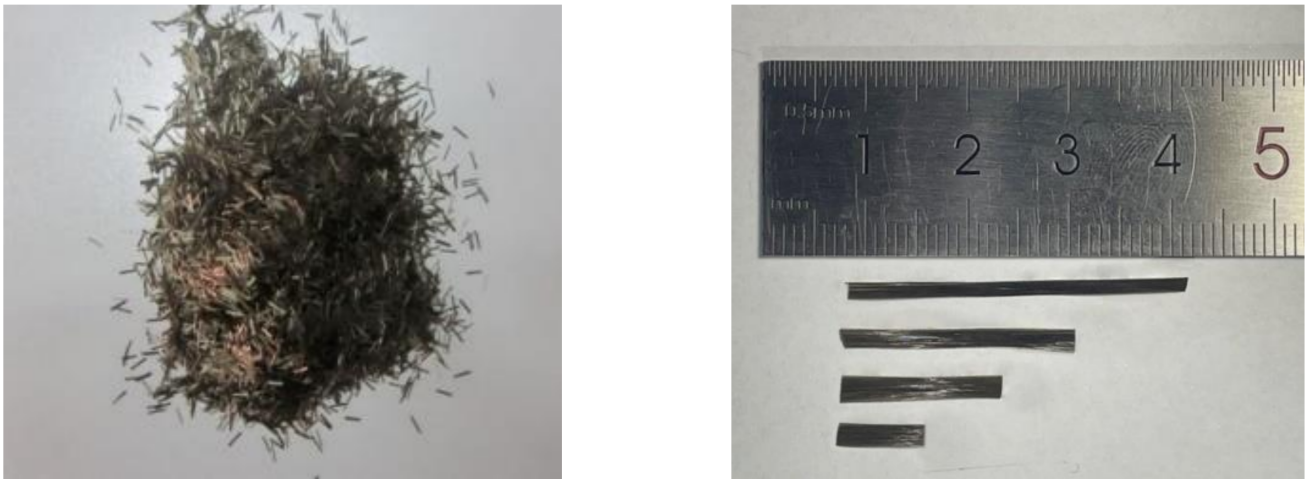

(**a**) Normal fibers (**b**) Fiber length

Figure 1. Basalt fibers.

Table 1. Physical properties of basalt fibers.

Property	Diameter, µm	Length, mm	Destiny, g·cm^{-3}	Tensile Strength, MPa	Melting Point, °C	Water Absorption, %	pH
Value	16	6/12/20/30	2.715	≥2000	1600	1.65	7.1

2.1.2. Asphalt

The asphalt binders used in this study were neat asphalt, SBS-modified asphalt, and rubber asphalt, the physical properties of which are presented in Tables 2–4.

Table 2. Physical properties of neat asphalt.

	Property	Acceptance Limits	Value	Test Method (JTG E20-2011) [34]
	Penetration (25 °C), 0.1 mm	60~80	74	T0604
	Softening point, °C	Min. 46	48.3	T0606
	Ductility (15 °C 5 cm/min), cm	Min. 100	>100	T0605
	PI	−1.5~1.0	−0.13	T0604
	Wax content, %	Max. 2.2	1.8	T0615
	Density (15 °C), g/cm^3	Measured	1.020	T0603
* RTFOT	Quality, %	Max. ±0.8	−0.05	T0610
	Penetration ratio (25 °C), %	Min. 61	74.0	T0604
	Ductility (15 °C), cm	Min. 15	23.9	T0605

* RTFOT: Rolling thin-film oven test.

Table 3. Physical properties of SBS-modified asphalt.

Property		Acceptance Limits	Value	Test Method (JTG E20-2011) [34]
Penetration (25 °C), 0.1 mm		60~80	69	T0604
Softening point, °C		Min. 55	64	T0606
Ductility (15 °C 5 cm/min), cm		Min. 30	48	T0605
PI		−0.4~1.0	0.5	T0604
Solubility (Trichloroethylene), %		Min. 99	99.8	T0607
Flash point, °C		Min. 230	329	T0611
Kinematic viscosity (235 °C), Pa·s		Max. 3	1.8	T0625
Elastic recovery (25 °C), %		Min. 65	76	T0662
Softening point difference, °C		Max. 2.5	1.4	T0661
* RTFOT	Quality, %	Max. ±1.0	−0.08	T0610
	Penetration ratio (25 °C), %	Min. 60	86	T0604
	Ductility (15 °C), cm	Min. 20	37	T0605

* RTFOT: Rolling thin-film oven test.

Table 4. Physical properties of rubber asphalt.

Property	Acceptance Limits	Value	Test Method (JTG E20-2011) [34]
Penetration (25 °C), 0.1 mm	30~60	53.7	T0604
Softening point, °C	Min. 60	64.0	T0606
Rotational viscosity (180 °C), Pa·s	2.0~5.0	2.510	T0625
Elastic recovery (25 °C), %	Min. 60	68	T0662
Ductility (5 °C), cm	Min. 5	7.1	T0605

2.2. Pull-Out Test

2.2.1. Pull-Out Equipment

The bond strength between basalt fibers and asphalt binders was measured using a pull-out tester (POT), which consists of a trial mold, a loading device, a temperature controller, and a wireless data control collector, as shown in Figure 2.

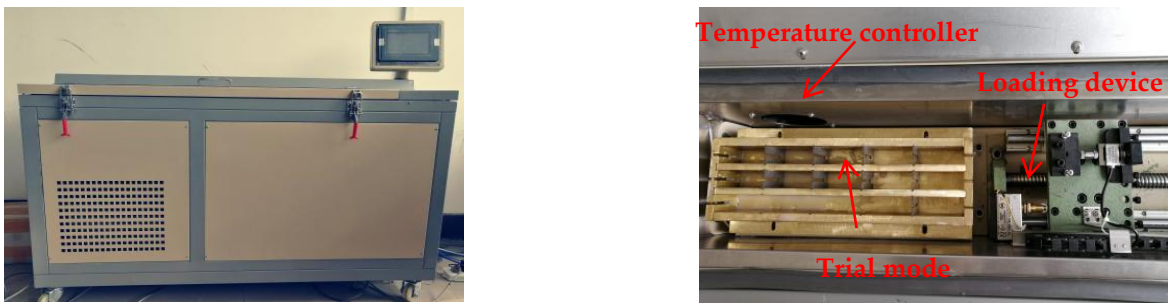

(**a**) The structure and parts of the POT.

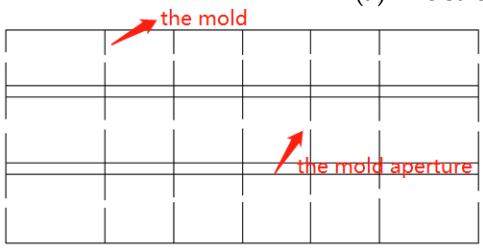

(**b**) The trial mold.

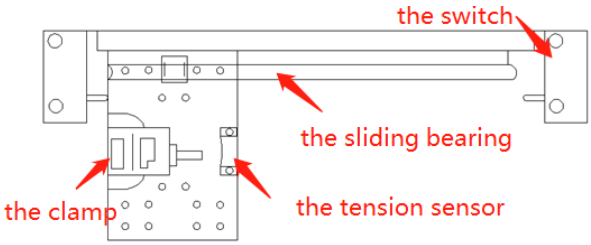

(**c**) The loading device.

Figure 2. *Cont.*



(**d**) The data collection system.

Figure 2. The pull-out tester.

2.2.2. Testing Procedure

The asphalt binders were prepared and heated at 150 °C (neat asphalt), 170 °C (SBS-modified asphalt), and 180 °C (rubber asphalt) to a fluid state. Then, half of the asphalt binders were poured into the trial mold carefully, and a bundle of BFs was placed into the gap. After that, the other half of the asphalt binders were poured into the trial mold, as shown in Figure 3. The specimens were placed in the POT at 60 °C for 1 h, and by this time, the loading device had been activated, operating at a speed of 10 mm/min.

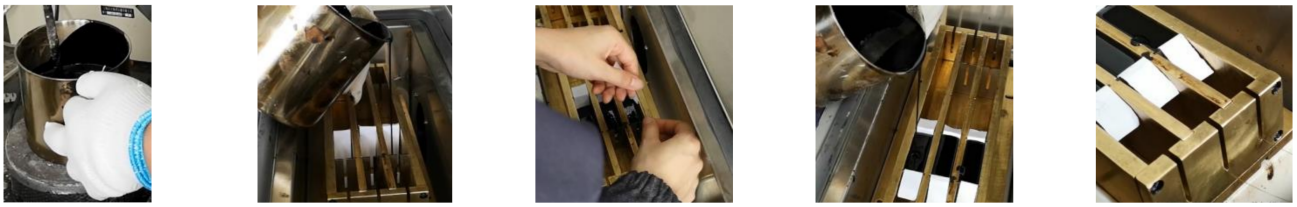

(**a**) (**b**) (**c**) (**d**) (**e**)

Figure 3. The procedures of the pull-out test. (**a**) Heating the asphalt binders. (**b**) Pouring the asphalt binders into the trial mold. (**c**) Placing a bundle of BFs into the gap. (**d**) Pouring asphalt binders left into the trial mold. (**e**) Completing the specimens for the POT.

The bond strength τ_m between BFs and asphalt binders was calculated according to Equation (1) using the maximum tensile force F_{max} measured using the POT (as shown in Figure 2) and the contact area S.

$$\tau_m = \frac{F_{max}}{S} \quad (1)$$

$$\mathrm{S} = 2(\mathrm{w} + \mathrm{h})\mathrm{L} \quad (2)$$

$$\mathrm{h} = 100\ \pi d^2/\mathrm{w} \quad (3)$$

where F_{max} is the maximum tensile force measured using the POT (as shown in Figure 2); S is the contact area; w is the width of fiber cross section; h is the embedment depth (the length of fiber in the asphalt binder) of the fibers; and d is the single-fiber diameter.

2.3. Contact Angle Test (CAT)

2.3.1. Surface Energy

The sessile drop method [35,36] is the most common and direct test used to measure the contact angle at 25 °C. The contact angle is an important parameter in evaluating the adhesion between materials, and its measurement allows the evaluation of solid surface free energy [37,38]. The relationship between surface energy and the contact angle is expressed in Young's equation [39,40].

$$\gamma_l \cos\theta = \gamma_s - \gamma_{sl} \quad (4)$$

where γ_l is the liquid surface free energy, θ is the contact angle, γ_s is the solid surface free energy, and γ_{sl} is the solid–liquid interfacial free energy (Figure 4).

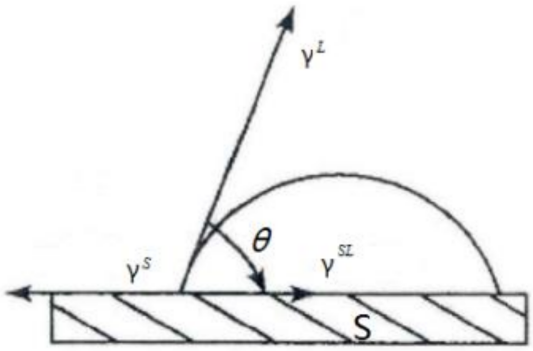

Figure 4. Contact angle test.

In this study, the dispersion components and the polar components were used to calculate the surface energy according to the equation derived by Owens and Wendt:

$$\frac{1+\cos\theta}{2}\frac{\gamma_l}{\sqrt{\gamma_l^d}} = \sqrt{\gamma_s^p} \times \sqrt{\frac{\gamma_l^p}{\gamma_l^d}} + \sqrt{\gamma_s^d} \quad (5)$$

$$\gamma_s = \gamma_s^p + \gamma_s^d \quad (6)$$

where γ_l^d is the dispersion component of the liquid surface free energy, γ_l^p is the polar component of the liquid surface free energy, γ_s is the solid surface free energy, γ_s^d is the dispersion component of the solid surface free energy, and γ_s^p is the polar component of the solid surface free energy.

2.3.2. Specimen Preparation for CAT

The asphalt binders were heated to 150 °C (neat asphalt), 170 °C (SBS-modified asphalt), and 180 °C (rubber asphalt) to obtain a fluid state, and then rectangular glass plates were placed into the asphalt binders vertically. After that, the glass plates with the asphalt binders were placed in an oven vertically until the excess asphalt binders flowed down to achieve the required film thickness. The specimens prepared as shown in Figure 5 were left for 24 h in a dryer at 25 °C before testing. The specimens were tested in four different parts.



Figure 5. Specimens for asphalt film.

2.4. Scanning Electron Microscopy

Scanning electron microscopy is a conventional technique used to study the microstructure of materials. Before preparation, BFs were placed in a drying oven at 105 °C and then premixed to maintain a good dispersion. Then, the asphalt binders were heated to 150 °C (neat asphalt), 170 °C (SBS-modified asphalt), and 180 °C (rubber asphalt), and basalt fibers were slowly added into the asphalt binders three times. In order to obtain a good distribution, the fiber–asphalt binders were stirred at a high speed of 1000 r/min for 30 min and then at 500 r/min for 20 min in a mixer. The specimens were sprayed

with gold for 15 min before testing. In this study, SEM images of the fiber–neat asphalt, fiber–SBS-modified asphalt, and fiber–rubber asphalt were examined to understand the microstructures of the fibers' dispersion in the asphalt binders.

3. Results and Analysis

3.1. Influence of Fiber Embedment Depths and Asphalt Binders on POT Results

Figures 6 and 7 show the maximum pull-out forces and bond strengths when BFs were added to the three different asphalt binders. The pull-out test also investigated the effects of the embedment depth of the basalt fibers on the bond strength between materials. Four embedment depths of basalt fibers (6 mm, 12 mm, 20 mm, and 30 mm) were selected in this test.

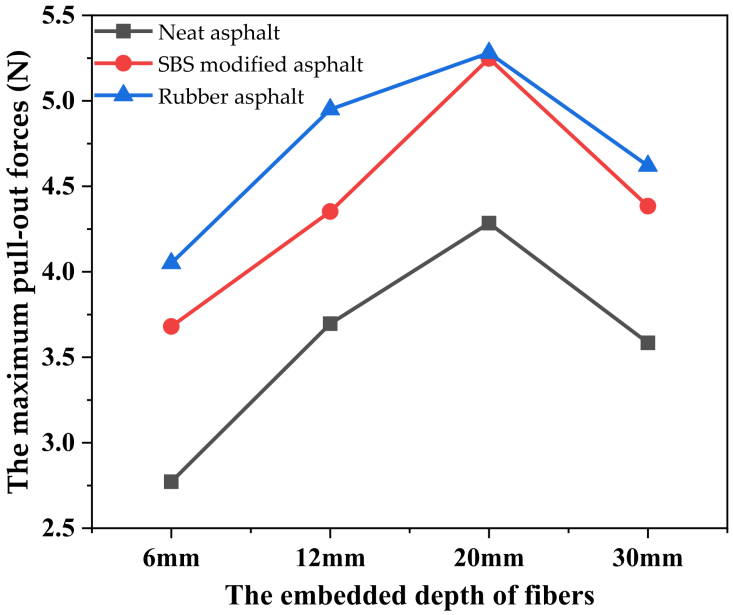

Figure 6. The maximum pull-out forces.

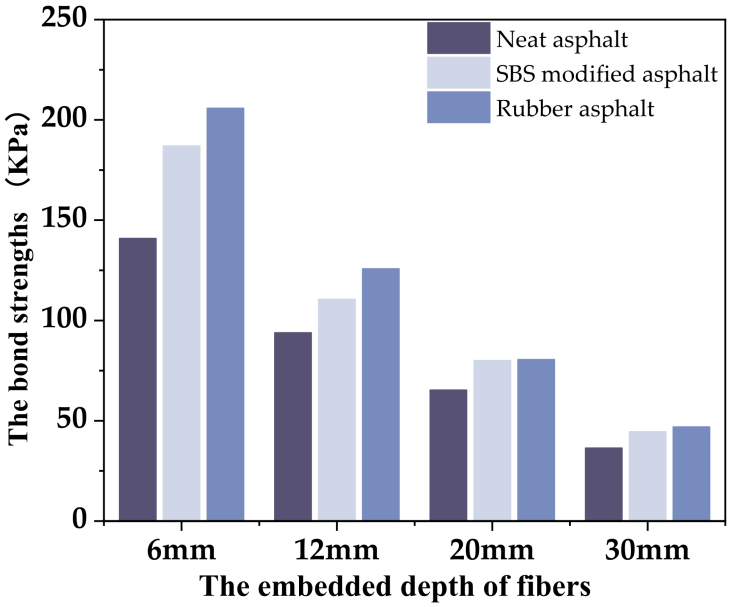

Figure 7. The bond strengths.

The pull-out forces increased rapidly at the beginning, indicating an increase in interfacial adhesion between the BFs and asphalt binders, so the bond strength of the

interface was gradually destroyed. When the bond failure of the interface extended to the ends of the embedded fibers, the tensile force acting on the fibers reached the maximum value. Then, the basalt fibers slid into the asphalt binders, and several fibers were pulled out from the asphalt binders. Therefore, there was a clear downtrend of pulling load in the bonding interface. When the pull-out test was carried out to a certain extent, the pull-out force of the fibers declined dramatically and tended to be relatively stable until the BFs were completely pulled out from the binders. It is obvious that the pull-out force of rubber asphalt with BFs was greater than that of neat asphalt and SBS-modified asphalt.

It was found that the pull-out force increased gradually with the increase in the embedment depth of the basalt fibers in the asphalt binders, but there was a decrease in the pull-out force when the embedment depth of the fibers exceeded a certain value. The optimal length of basalt fibers (20 mm) can be obtained by referring to Figure 6. These results suggest that increasing the embedment depth of basalt fibers to a certain level can improve the mechanical properties of fiber–asphalt binders. The performance of asphalt binders is adversely affected if the fiber length is too long or too short. When basalt fibers are used in HMA, the length of basalt fibers is restricted by the effects of asphalt binders.

Figure 7 shows that the bond strength between basalt fibers and asphalt binders differs based on the asphalt binder: rubber asphalt > SBS-modified asphalt > neat asphalt. This suggests that the bond strength between basalt fibers and asphalt binders is directly affected by the compatibility between them and the properties of the asphalt binders.

3.2. Scanning Electron Micrograph

The microstructures of the BFs exhibited in the SEM images are presented in Figure 8. The images reveal that the fibers are round with small protruding dots, indicating that they are capable of absorbing a certain amount of asphalt binder.

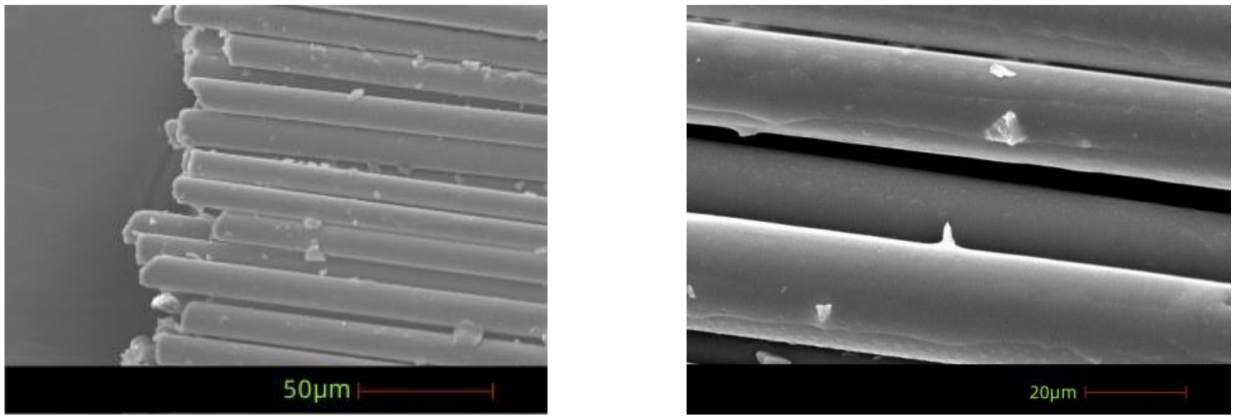

Figure 8. The SEM images of BFs.

An SEM image of the fiber–asphalt binders is shown in Figure 9. The bright portion of the image represents the dispersed fibers, while the dark portion indicates the asphalt binders. These uniformly distributed portions demonstrate that the fibers and asphalt binders were effectively combined, and the asphalt binders cover the fibers' surfaces evenly, proving that BFs have good absorption capability. SEM images of the damaged surfaces of the basalt fiber–asphalt binders are shown in Figure 10. The asphalt binders adhered to the surfaces of the BFs and formed tentacles surrounding them, exerting an interlocking effect on the materials and enhancing the adhesion and bond strength between the materials. BFs are dispersed in asphalt binders and form a spatial network structure overlapping each other. So, BFs act as a bridge, cracking when the HMA bears a load, and they can effectively prevent and slow down the relative slip of asphalt and aggregate and solve the problem of stress concentration.

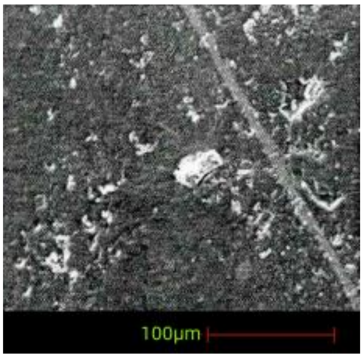

Figure 9. Asphalt binders with BFs.

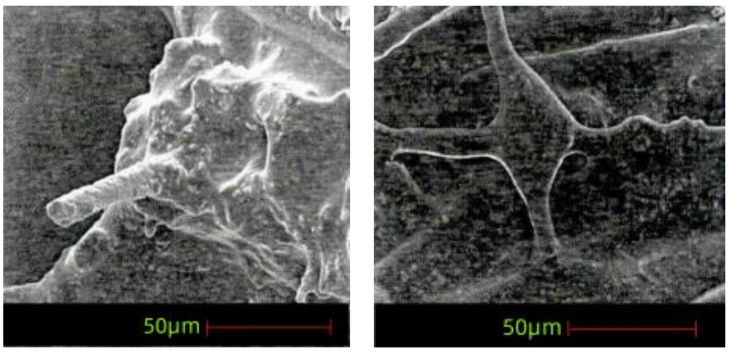

Figure 10. Damaged surface topography of asphalt binders with BFs.

3.3. Surface Energy and Contact Angle

3.3.1. Surface Energy Calculation of Asphalt

The selection of appropriate probe liquids is important to determine surface energy using the sessile drop method. For a liquid to be used as a probe, it should have good stability and high surface free energy and be immiscible with the asphalt binders. Distilled water, ethylene glycol, and formamide were selected from the literature as probe liquids for the surface energy calculation. The surface energy characteristics of the probe liquids used in the contact angle experiments and analyses are summarized in Table 5.

Table 5. Surface energy of probe liquids (25 °C).

Test Liquid Type	Surface Energy and Its Component (mJ/m^2)		
	γ_l	γ_l^d	γ_l^p
Distilled water	72.8	21.8	51
Ethylene glycol	48	29	19
Formamide	58	39	19

Table 6 shows the contact angle measurements between the asphalt types and probe liquids. It shows that the standard deviations over the mean (SD) are very low, with a maximum value of 0.56%.

Table 6. Sessile drop results for asphalt mortar.

Asphalt Type	Distilled Water		Ethylene Glycol		Formamide	
	Contact Angle (°)	SD	Contact Angle (°)	SD	Contact Angle (°)	SD
Neat asphalt	101.6	0.28	93.3	0.56	84.9	0.35
SBS-modified asphalt	96.2	0.37	87.7	0.52	76.9	0.41
Rubber asphalt	89.4	0.31	76.7	0.51	68.9	0.38

According to the contact angles of the probe liquids with asphalt binders and the respective surface energy, by substituting Equation (5) to establish a system of equations, we could obtain the surface energy and relevant components of the neat asphalt, SBS-modified asphalt, and rubber asphalt, as shown in Table 7.

Table 7. Asphalt surface energy and its component (mJ/m^2).

Asphalt Binders	γ_s	γ_s^d	γ_s^p
Neat asphalt	18.58	16.59	1.99
SBS-modified asphalt	23.82	21.53	2.29
Rubber asphalt	28.57	25.04	3.53

The table above shows that the surface energy of rubber asphalt is greater than those of the other two, indicating that the intermolecular force of rubber asphalt is stronger. The dispersion component accounts for more surface free energy of asphalt than the polar component. It is believed that the main component of asphalt binders is a non-polar hydrocarbon.

3.3.2. Surface Energy Calculation for BFs

The surface energy of BFs was determined by using the same method as that used for asphalt binders. The BFs were placed in an oven at 105 °C for 3 h before testing and then transferred to a desiccator.

During the test, the BFs were symmetrically clamped and fixed on the sample holder, moved at a speed of 0.008 mm/s, and slowly immersed into the two test liquids. The surface energy γ_s of the BFs and the non-polar part γ_s^d and the polar part γ_s^p were obtained using the Owens–Wendt equation, and the results are listed in Table 8. Distilled water and ethylene glycol were used as the test liquids in this test.

Table 8. Surface energy of BFs.

Type	Contact Angle with Liquid (°)		Surface Energy and Its Component (mJ/m^2)		
	Distilled Water	Ethylene Glycol	γ_s	γ_s^d	γ_s^p
BFs	71.103 ± 8.305	39.594 ± 5.074	37.98	11.39	26.61

3.3.3. Adhesion Work of Asphalt Binders and Basalt Fibers

The thermodynamic adsorption theory states that adhesion occurs under conditions of sufficient moisture. According to the basic theory of surface energy, the contact angle and adhesion work can be used as an index of the adhesion between asphalt binders and BFs. The adhesion work represents the bonding ability between asphalt binders and BFs. Generally, the adhesion work of two materials is expressed by Equation (4). The basic theory of surface energy indicates that the adhesion work and Gibbs free energy are opposite to each other, and the adhesion work is not less than zero, which means that the adhesion process can occur spontaneously.

$$W_a = \gamma_l + \gamma_s - \gamma_{sl} \quad (7)$$

According to Van der Waals theory and Lewis acid–base theory, if the small force between molecules is neglected, the adhesion work can be expressed by their dispersion component and polar component, as shown in Equation (5).

$$W_a = 2\sqrt{\gamma_s^d \gamma_l^d} + 2\sqrt{\gamma_s^p \gamma_l^p} \quad (8)$$

The rubber asphalt with BFs showed a higher value of adhesion work (53.160 mJ/m^2) compared to that of the neat asphalt (42.046 mJ/m^2) and SBS-modified asphalt (46.932 mJ/m^2)

with BFs. Rubber asphalt is more suitable as a binder for basalt fibers, and this is consistent with the results of POT.

3.4. Comprehensive Analysis of Bond Strength Based on the Grey Relational Method

In this paper, the fiber embedment depth and asphalt softening point were chosen. The Gray relational method was employed according to the data (as shown in Table 9) on the bond strength of fibers at embedment depths of 6, 12, 20, and 30 mm and asphalt types of neat asphalt, SBS-modified asphalt, and rubber asphalt [41]. The reason for using the softening point data to represent the asphalt is that penetration corresponds to viscosity, which correlates precisely with the bond strength of the fiber asphalt. The correlation of bond strength with fiber embedment depth and asphalt softening point (denoted as $A_{embedded\ depth}$ and $A_{asphalt}$) was determined according to the grey relational method. The data in each row were divided simultaneously by the data in the first row according to the normalization method. After choosing the bond strength as the reference series, the correlation coefficients of basalt fibers were calculated according to the correlation coefficient calculation method. Finally, the correlation of fiber bond strength was obtained by averaging the correlation coefficients of each row between each indicator. The correlation of the bond strength of the fibers with fiber embedment depth is $A_{embedded\ depth}$ (0.5901). The correlation of the bond strength of the fibers with asphalt softening point is $A_{asphalt}$ (0.8318).

Table 9. The data obtained using the grey relational method.

Bond Strengths/kPa	Embedment Depth/mm	Softening Point
140.8869	6	74
93.92458	12	74
65.32027	20	74
36.43135	30	74
187.036	6	69
110.5952	12	69
80.01886	20	69
44.56335	30	69
205.8412	6	53.7
125.7918	12	53.7
80.50678	20	53.7
46.96229	30	53.7

By comparing the correlations, it can be seen that the factors influencing bond strength were ranked as follows: $A_{asphalt} > A_{embedded\ depth}$. The bond strength of the basalt fibers with asphalt binder was determined by the physicochemical properties of the fibers and the asphalt binder. And the change in the type of asphalt binder led to a change in the interfacial contact property between the fibers and asphalt binder. Therefore, the bond strength between basalt fibers and asphalt binder was highly dependent on the type of asphalt binder.

4. Conclusions

In this study, the bond strength between basalt fibers (BFs) and asphalt binders was investigated using a pull-out tester. Based on the test results and the discussion above, the following conclusions can be drawn:

1. Appropriate embedment depths of BFs are beneficial to the bonding strength between basalt fibers and asphalt binders, which can further guide the selection of basalt fiber length. In addition, rubber asphalt has a higher bond strength with basalt fibers than the other two asphalts.
2. The types of asphalt binders suitable for basalt fibers and the appropriate fiber embedding depths for different types of asphalt binders guiding the selection of fiber length were recommended based on the influence of the fiber embedding depth and

asphalt binders on fiber–asphalt bonding strength. The recommended fiber length is 20 mm. The recommended asphalt type is rubber asphalt.

3. SEM images revealed the uniform distribution of fibers in the asphalt binders and the spatial networks of basalt fibers in the asphalt binders.
4. The surface energy of the asphalt binders and basalt fibers showed that rubber asphalt with BFs had good adhesivity and high homogeneity.
5. The results obtained using the gray correlation method showed that bond strength correlates more closely with the type of asphalt binder than embedment depth.
6. Finally, further research is required to investigate the distribution of basalt fibers in asphalt binders. In this study, a preliminary analysis of the microscopic mechanism of BFs in asphalt binders was carried out. The microscopic mechanisms of basalt fibers–asphalt binders also need to be further analyzed.

Author Contributions: Conceptualization, C.K. and A.K.; Methodology, C.K., A.K. and P.X.; Formal analysis, Y.L.; Investigation, Y.L.; Resources, Z.W.; Data curation, Y.L.; Writing—original draft, Z.S.; Writing—review & editing, Z.S. and C.K.; Supervision, Z.W. and P.X.; Project administration, C.K., Z.W., A.K. and P.X.; Funding acquisition, C.K., Z.W., A.K. and P.X. All authors have read and agreed to the published version of the manuscript.

Funding: The financial support was provided by the National Natural Science Foundation of China (Grant Number: 52178439), the Natural Science Foundation for Youths of Jiangsu Province (Grant Number: BK20190913), the Yangzhou University High-level Talent Support Program, the Postgraduate Research & Practice Innovation Program of Jiangsu Province (Yangzhou University; SJCX22_1746), the Jiangsu Science and Technology Association Promotion Project for the Youths (Grant Number: 2021-090), and the Qing Lan Project of Jiangsu Province.

Institutional Review Board Statement: Not applicable.

Informed Consent Statement: Not applicable.

Data Availability Statement: The data presented in this study are available on request from the corresponding author due to privacy.

Acknowledgments: We would like to thank the Testing Center of Yangzhou University for their technical support.

Conflicts of Interest: The authors declare no conflict of interest.

References

1. Li, Z.; Li, K.; Chen, W.; Liu, W.; Yin, Y.; Cong, P. Investigation on the characteristics and effect of plant fibers on the properties of asphalt binders. *Constr. Build. Mater.* **2022**, *338*, 127652. [CrossRef]
2. Zhang, X.; Chen, E.; Li, N.; Wang, L.; Si, C.; Wang, C. Micromechanical analysis of the rutting evolution of asphalt pavement under temperature–stress coupling based on the discrete element method. *Constr. Build. Mater.* **2022**, *325*, 126800. [CrossRef]
3. Li, D.; Leng, Z.; Zhang, S.; Jiang, J.; Yu, H.; Wellner, F.; Leischner, S. Blending efficiency of reclaimed asphalt rubber pavement mixture and its correlation with cracking resistance. *Resour. Conserv. Recycl.* **2022**, *185*, 106506. [CrossRef]
4. Xu, O.; Li, Y.; Xu, R.; Liu, Y.; Dong, Y. Performance evaluation of waterborne epoxy resin modified emulsified asphalt mixtures for asphalt pavement pothole repair. *Constr. Build. Mater.* **2022**, *325*, 126709. [CrossRef]
5. Wang, S.; Sui, X.; Leng, Z.; Jiang, J.; Lu, G. Asphalt pavement density measurement using non-destructive testing methods: Current practices, challenges, and future vision. *Constr. Build. Mater.* **2022**, *344*, 128154. [CrossRef]
6. Ghuzlan, K.A.; Bara, W.A.M.; Al-Momani, A.S. Rutting performance of asphalt mixtures with gradations designed using Bailey and conventional Superpave methods. *Constr. Build. Mater.* **2020**, *261*, 119941. [CrossRef]
7. Zhou, X.; Zhao, G.; Tighe, S.; Chen, M.; Wu, S.; Adhikari, S.; Gao, Y. Quantitative comparison of surface and interface adhesive properties of fine aggregate asphalt mixtures composed of basalt, steel slag, and andesite. *Constr. Build. Mater.* **2020**, *246*, 118507. [CrossRef]
8. Cui, S.; Sheng, Y.; Wang, Z.; Jia, H.; Qiu, W.; Temitope, A.A.; Xu, Z. Effect of the fiber surface treatment on the mechanical performance of bamboo fiber modified asphalt binder. *Constr. Build. Mater.* **2022**, *347*, 128453. [CrossRef]
9. Chu, H.H.; Almohana, A.I.; QasMarrogy, G.A.; Almojil, S.F.; Alali, A.F.; Almoalimi, K.T.; Raise, A. Experimental investigation of performance properties of asphalt binder and stone matrix asphalt mixture using waste material and warm mix additive. *Constr. Build. Mater.* **2023**, *368*, 130397. [CrossRef]

10. Slebi-Acevedo, C.J.; Lastra-González, P.; Pascual-Muñoz, P.; Castro-Fresno, D. Mechanical performance of fibers in hot mix asphalt: A review. *Constr. Build. Mater.* **2019**, *200*, 756–769. [CrossRef]
11. Li, Z.; Shen, A.; Wang, H.; Guo, Y.; Wu, H. Effect of basalt fiber on the low-temperature performance of an asphalt mixture in a heavily frozen area. *Constr. Build. Mater.* **2020**, *253*, 119080. [CrossRef]
12. Davar, A.; Tanzadeh, J.; Fadaee, O. Experimental evaluation of the basalt fibers and diatomite powder compound on enhanced fatigue life and tensile strength of hot mix asphalt at low temperatures. *Constr. Build. Mater.* **2017**, *153*, 238–246. [CrossRef]
13. Katkhuda, H.; Shatarat, N. Improving the mechanical properties of recycled concrete aggregate using chopped basalt fibers and acid treatment. *Constr. Build. Mater.* **2017**, *140*, 328–335. [CrossRef]
14. Alnahhal, W.; Aljidda, O. Flexural behavior of basalt fiber reinforced concrete beams with recycled concrete coarse aggregates. *Constr. Build. Mater.* **2018**, *169*, 165–178. [CrossRef]
15. Xie, T.; Wang, L. Optimize the design by evaluating the performance of asphalt mastic reinforced with different basalt fiber lengths and contents. *Constr. Build. Mater.* **2023**, *363*, 129698. [CrossRef]
16. Gu, Q.; Kang, A.; Li, B.; Xiao, P.; Ding, H. Effect of fiber characteristic parameters on the high and low temperature rheological properties of basalt fiber modified asphalt mortar. *Case Stud. Constr. Mater.* **2022**, *17*, e01247. [CrossRef]
17. Lou, K.; Xiao, P.; Kang, A.; Wu, Z.; Li, B.; Lu, P. Performance evaluation and adaptability optimization of hot mix asphalt reinforced by mixed lengths basalt fibers. *Constr. Build. Mater.* **2021**, *292*, 123373. [CrossRef]
18. Qin, X.; Shen, A.; Guo, Y.; Li, Z.; Lv, Z. Characterization of asphalt mastics reinforced with basalt fibers. *Constr. Build. Mater.* **2018**, *159*, 508–516. [CrossRef]
19. Khan, M.; Cao, M.; Ali, M. Effect of basalt fibers on mechanical properties of calcium carbonate whisker-steel fiber reinforced concrete. *Constr. Build. Mater.* **2018**, *192*, 742–753. [CrossRef]
20. Kathari, P.M.; Sandra, A.K.; Sravana, P. Experimental investigation on the performance of asphalt binders reinforced with basalt fibers. *Innov. Infrastruct. Solut.* **2018**, *3*, 76. [CrossRef]
21. Lou, K.; Xiao, P.; Tang, Q.; Wu, Y.; Wu, Z.; Pan, X. Research on the micro-nano characteristic of basalt fiber and its impact on the performance of relevant asphalt mastic. *Constr. Build. Mater.* **2022**, *318*, 126048. [CrossRef]
22. Wu, B.; Pei, Z.; Luo, C.; Xia, J.; Chen, C.; Kang, A. Effect of different basalt fibers on the rheological behavior of asphalt mastic. *Constr. Build. Mater.* **2022**, *318*, 125718. [CrossRef]
23. Wang, D.; Wang, L.; Gu, X.; Zhou, G. Effect of basalt fiber on the asphalt binder and mastic at low temperature. *J. Mater. Civ. Eng.* **2013**, *25*, 355–364. [CrossRef]
24. Fu, Z.; Tang, Y.; Ma, F.; Wang, Y.; Shi, K.; Dai, J.; Hou, Y.; Li, J. Rheological properties of asphalt binder modified by nano-TiO_2/ZnO and basalt fiber. *Constr. Build. Mater.* **2022**, *320*, 126323. [CrossRef]
25. Cheng, X.; Liu, J.; Han, C.; Zhang, X.; Wu, Z. Silane coupling agent impact on surface features of modification of basalt fibers and the rheological properties of basalt fiber reinforced asphalt. *Constr. Build. Mater.* **2023**, *366*, 130182. [CrossRef]
26. Mohammed, M.; Parry, T.; Thom, N.; Grenfell, J. Investigation into the bond strength of bitumen-fibre mastic. *Constr. Build. Mater.* **2018**, *190*, 382–391. [CrossRef]
27. Rahim, A.; Thom, N.; Airey, G. Development of compression pull-off test (CPOT) to assess bond strength of bitumen. *Constr. Build. Mater.* **2019**, *207*, 412–421. [CrossRef]
28. Zhang, X.; Gu, X.; Lv, J.; Zhu, Z.; Ni, F. Mechanism and behavior of fiber-reinforced asphalt mastic at high temperature. *Int. J. Pavement Eng.* **2018**, *19*, 407–415. [CrossRef]
29. Zhang, X.; Gu, X.; Lv, J.; Zhu, Z.; Zou, X. Numerical analysis of the rheological behaviors of basalt fiber reinforced asphalt mortar using ABAQUS. *Constr. Build. Mater.* **2017**, *157*, 392–401. [CrossRef]
30. Kou, C.; Chen, Z.; Kang, A.; Zhang, M.; Wang, R. Rheological behaviors of asphalt binders reinforced by various fibers. *Constr. Build. Mater.* **2022**, *323*, 126626. [CrossRef]
31. Cui, B.; Wang, H.; Gu, X.; Hu, D. Study of the inter-diffusion characteristics and cracking resistance of virgin-aged asphalt binders using molecular dynamics simulation. *Constr. Build. Mater.* **2022**, *351*, 128968. [CrossRef]
32. Gajewski, M.; Bańkowski, W.; Gajewska, B.; Sybilski, D.; Horodecka, R. Estimation of asphalt binders' resistance to permanent deformation with application of the MSCR and multiple shear creep long recovery (MSCLR) tests. *Constr. Build. Mater.* **2021**, *284*, 122808. [CrossRef]
33. Guo, F.; Li, R.; Lu, S.; Bi, Y.; He, H. Evaluation of the effect of fiber type, length, and content on asphalt properties and asphalt mixture performance. *Materials* **2020**, *13*, 1556. [CrossRef] [PubMed]
34. *JTG E20-2011*; Standard Test Methods of Bitumen and Bituminous Mixtures for Highway Engineering. Occupation Standard of the People's Republic of China: Beijing, China, 2011.
35. Espinal, M.; Kane, S.; Ryan, C.; Phillips, A.; Heveran, C. Evaluation of the bonding properties between low-value plastic fibers treated with microbially-induced calcium carbonate precipitation and cement mortar. *Constr. Build. Mater.* **2022**, *357*, 129331. [CrossRef]
36. Moraes, R.; Velasquez, R.; Bahia, H. Using bond strength and surface energy to estimate moisture resistance of asphalt-aggregate systems. *Constr. Build. Mater.* **2017**, *130*, 156–170. [CrossRef]
37. Liu, Y.; Zhang, Z.; Tan, L.; Xu, Y.; Wang, C.; Liu, P.; Yu, H.; Oeser, M. Laboratory evaluation of emulsified asphalt reinforced with glass fiber treated with different methods. *J. Clean. Prod.* **2020**, *274*, 123116. [CrossRef]

38. Park, P.; El-Tawil, S.; Naaman, A.E. Pull-out behavior of straight steel fibers from asphalt binder. *Constr. Build. Mater.* **2017**, *144*, 125–137. [CrossRef]
39. Noorvand, H.; Mobasher, B.; Underwood, S.; Kaloush, K. Development of an analytical framework for evaluation of critical fiber length in asphalt concrete with a fiber pullout test. *Constr. Build. Mater.* **2022**, *360*, 129561. [CrossRef]
40. Teklal, F.; Djebbar, A.; Allaoui, S.; Hivet, G.; Joliff, Y.; Kacimi, B. A review of analytical models to describe pull-out behavior–Fiber/matrix adhesion. *Compos. Struct.* **2018**, *201*, 791–815. [CrossRef]
41. Zhang, Y.; Wang, Y.; Kang, A.; Wu, Z.; Li, B.; Zhang, C.; Wu, Z. Analysis of Rejuvenating Fiber Asphalt Mixtures' Performance and Economic Aspects in High-Temperature Moisture Susceptibility. *Materials* **2022**, *15*, 7728. [CrossRef] [PubMed]

Disclaimer/Publisher's Note: The statements, opinions and data contained in all publications are solely those of the individual author(s) and contributor(s) and not of MDPI and/or the editor(s). MDPI and/or the editor(s) disclaim responsibility for any injury to people or property resulting from any ideas, methods, instructions or products referred to in the content.